

Sensing-area distribution functions for one- and three-loop superconductive magnetic-monopole detectors

B. Cabrera, R. Gardner, and R. King

Department of Physics, Stanford University, Stanford, California 94305-2196

(Received 2 January 1985)

We have calculated the response of the existing one- and three-loop superconductive magnetic-monopole detectors to an isotropic distribution of monopole trajectories passing through the detectors. The effective sensing area of the three-loop detector is shown to be 476 cm^2 for events greater than $0.1\Phi_0$ ($\Phi_0 = hc/2e$) in at least two of the three loops. These calculations include the effects of the cylindrical superconducting shields surrounding the loops. First the interior magnetic-field distribution within the cylindrical shield is found for a doubly quantized vortex located in the shield wall. Next the coupling of this field to each superconducting loop is computed as a function of the position of the vortex relative to the loop. Then the current change induced in the loops is found for each monopole trajectory by combining the direct coupling to the entering and exiting cylinder wall vortices. The one- and three-loop sensing-area distribution functions are then found using a Monte Carlo technique on a large number of isotropically distributed trajectories.

I. INTRODUCTION

Grand unification theories predict the existence of stable supermassive magnetically charged particles possessing the Dirac unit of magnetic charge.¹ These particles would be nonrelativistic, weakly ionizing, and extremely penetrating; and thus there may exist a cosmic-ray flux of such particles which has eluded previous searches. The theoretical similarities between flux quantization in superconductors and Dirac magnetic monopoles make superconductive systems natural detectors in searches for these elusive particles. The total magnetic flux emanating from a single Dirac charge g is exactly two flux quanta Φ_0 ,

$$4\pi g = hc/e = 2\Phi_0. \quad (1)$$

The passage of a Dirac magnetic charge through a superconducting ring would induce a current change in the ring corresponding to a flux change of exactly $2\Phi_0$.

Two such detectors have been built in our laboratory. The first, a prototype single-loop device² consisting of a four-turn 5.1-cm-diameter loop made of 0.005-cm-diameter niobium wire, was operated as a monopole detector for 382 days. A single candidate event was observed, but it has not been possible to rule out a spurious cause. Thus a second detector³ has been built which is based on the same principles as the prototype device but with improved mechanical stability, a greater sensing area, and much better spurious-signal discrimination. It consists of three mutually orthogonal superconducting loops, each 10.2 cm in diameter and made of two turns of 0.013-cm-diameter niobium titanium wire. This new detector has been in operation for over 18 months.

The passage of a single Dirac charge through the loops of these detectors would result in $2\Phi_0$ coupling to each turn of the loops (a total of $8\Phi_0$ for the prototype device and of $4\Phi_0$ for each loop of the larger device). No change

results for a particle trajectory which misses the loop. This simple response is more complicated in practice because the loops are mounted inside of superconducting shields to isolate them from ambient magnetic field changes which could also couple to the loops. Thus, in addition to the trajectory coupling directly to the loop, doubly quantized supercurrent vortices appear in the walls of the shield at the points where the particle trajectory enters and exits. These vortices produce a change in the magnetic field within the shield which also couples to the loops, even if the trajectory itself misses the loops. Thus the possible values for the total current induced in the loop are no longer sharp, depending only on whether the trajectory passed through the loop, but now form a continuous range of values which depend on the exact trajectory through the shield.

In this paper we summarize calculations which completely characterize the response of the two superconductive detectors to an isotropic distribution of magnetic-monopole trajectories. Section II describes the idealized detector models we use for our calculations. In Sec. III we explicitly compute the magnetic field inside of the cylindrical shield produced by one doubly quantized vortex in the wall. The coupling of this field to each detector loop is then found as a function of the vortex position with respect to the loop (Sec. IV) for both the one- and three-loop detectors. Using a Monte Carlo technique, the density of sensing-area distribution functions are found for both detectors in Sec. V. The applicability of these results to the actual detector sensitivities and effective sensing areas is discussed in Sec. VI.

II. THE DETECTOR MODELS

To characterize the response of these detectors to the passage of a magnetic charge we have used idealized exact models. As we discuss below in Sec. VI, the differences between these models and the actual detectors have only a

small effect on the results.

The prototype detector consists of a four-turn loop of niobium wire with its axis vertical and coincident with that of a cylindrical superconducting shield. The radius of the loop is 2.54 cm and that of the shield is 10.16 cm. The length of the shield is 1 m and the loop is located 72 cm from the open top (the bottom of the shield is closed). The loop is connected to the superconducting input coil of a SQUID (superconducting quantum interference device) magnetometer which continuously monitors the loop supercurrent. The passage of a single Dirac charge through the loop would result in an $8\Phi_0$ change in the flux through the superconducting circuit, comprised of the detection loop and SQUID input coil. The supercurrent itself changes by about 4 nA, 40 times greater than the detector noise band.

In our model for the prototype detector, shown in Fig. 1(a), we take an infinite cylinder of radius $A = 10.16$ cm surrounding a coaxial loop of radius $A/4$. Portions of the shield further than one diameter from the loop do not contribute significantly, and thus it is not necessary to consider the exact shield geometry. We choose the z axis to be coincident with the shield axis and the origin of our spherical coordinates to be coincident with the center of the loop plane. This detector is azimuthally symmetric.

The larger three-loop detector is mounted in an identical superconducting shield to the one used for the prototype detector. Each loop is 5.08 cm in radius and made of two turns of 0.013-cm-diameter niobium wire. The three loops are connected to independent SQUID magnetometers, each monitoring the current of one loop. A $4\Phi_0$ change in the flux would result from the passage of a Dirac charge through any loop of this detector. The loops are wound on a spherical bulb with their planes mutually orthogonal. The $(1,1,1)$ direction in a coordinate system made up of the three loop normals is coincident with the axis of the shield, so the angle between the shield axis and each loop normal is

$$\theta_0 = \arccos(1/\sqrt{3}) = 50^\circ 44' 8.20''.$$

The model for the three-loop detector, shown in Fig. 1(b), also uses an infinite cylinder of radius $A = 10.16$ cm to model the shield and each loop has radius $A/2$. Again the z direction is taken along the shield axis and the polar angle θ measured down from the shield axis and centered at the three-loop center. An azimuthal coordinate ϕ is also required and is measured from the symmetry plane through loop 1 on the side closest to the upward-pointing loop normal in a counterclockwise direction about the cylinder axis. The normals to loops 2 and 3 are located at $\phi = 2\pi/3$ and $4\pi/3$, respectively. The three-loop system within the shield possesses twelvefold symmetry which is derived from the twofold reflection symmetry about the symmetry plane of each loop ($\phi = 0$ plane for loop 1), from the threefold rotational symmetry about the cylinder axis and from inversion symmetry through the coordinate origin. These symmetries greatly simplify the calculations.

The passage of a monopole of charge q_g through these detectors would change the supercurrent in the loops in two ways. First, if the monopole passes through one of

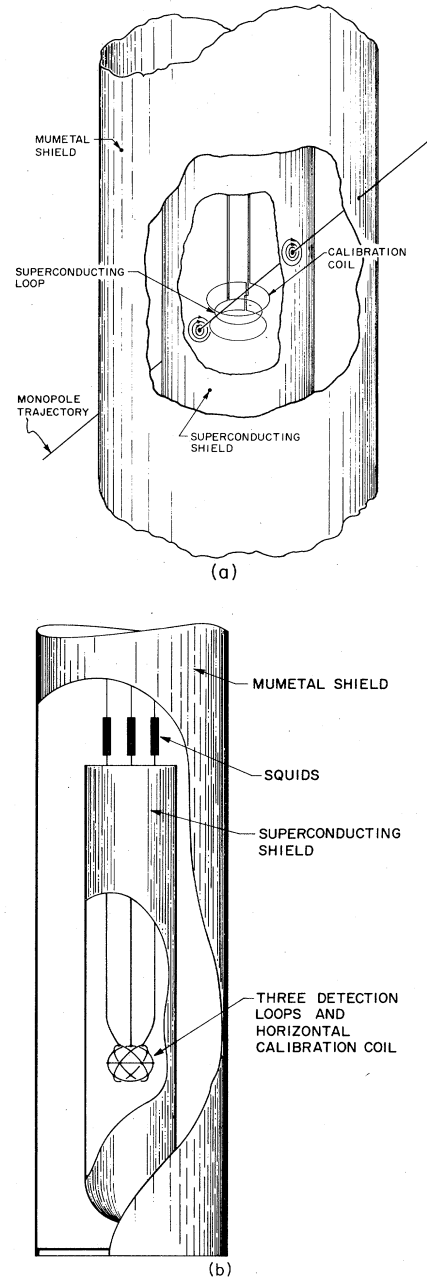


FIG. 1. Schematics of (a) single-loop detector and (b) three-loop detector.

the loops, in the direction of the loop normal, it would produce a flux change $\Delta\Phi = -4\pi q_g N$, where N is the number of loop turns. For a Dirac charge g , $4\pi g = 2\Phi_0$, so that a flux change of exactly $2\Phi_0$ per turn would result. Second, at the point on the shield wall where the monopole enters the lead cylinder, it would produce a supercurrent vortex in the superconducting lead. The monopole would leave a second vortex at its exit point on the cylinder wall. The magnetic flux through each of these current vortices is also $2\Phi_0$ and for a positive charge the

magnetic field would point outwards at the trajectory entrance and inwards at the exit. These vortices in the wall produce a magnetic-flux change $\Delta\Phi_{\text{vor}}$ across each loop whether or not the trajectory passes through that loop. The perfectly diamagnetic response of the superconducting ring results in an induced supercurrent change

$$\Delta I = -N \Delta\Phi_{\text{vor}}/L,$$

where L is the total self-inductance of the closed superconducting circuit made up of the loop and SQUID input coil. This second supercurrent change usually opposes the first and never changes the total flux through the loop. Only the passage of the charge directly through the loop changes the flux, by a quantized amount. However, these detectors measure the supercurrent change and not the total flux change.

As we shall see, it is convenient in the calculations that follow to write $\Delta\Phi_{\text{vor}}$ as

$$\begin{aligned} \Delta\Phi_{\text{vor}} &= 4\pi q_g (f_{\text{in}} - f_{\text{out}}), \\ f_{\text{in}} &= f(\phi_{\text{in}}, z_{\text{in}}), \\ f_{\text{out}} &= f(\phi_{\text{out}}, z_{\text{out}}), \end{aligned} \quad (2)$$

where $-1 < f(\phi, z) < 1$ is the fraction of the total flux from the vortex coupling to the loop. The vortex is taken to have its magnetic field pointing outward and is located at (ϕ, z) in the loop coordinates. Half of the flux leaving at (ϕ, z) enters from infinity at the cylinder top and half from below at the bottom. The negative sign in front of f_{out} describes an oppositely pointing vortex at the exit. Thus the total supercurrent change through a loop produced by the passage of a magnetic charge q_g can be written as

$$\Delta I = -(4\pi q_g N/L)(\eta - f_{\text{in}} + f_{\text{out}}), \quad (3)$$

where $\eta = +1$ if the trajectory intersects the loop in the direction of the loop normal, $\eta = -1$ if it intersects in the opposite sense, and $\eta = 0$ if it misses the loop. We will always express ΔI in units of Φ_0/L . To find f , we first must calculate the field from a single wall vortex inside of the infinite superconducting cylinder (next section), and then perform a surface integral across the loop surface, for each different vortex location (Sec. IV).

III. MAGNETIC FIELD FROM VORTEX ON WALL

Since there are no currents flowing inside of the superconducting cylinder but only in the walls, $\nabla \times \mathbf{B} = 0$ and we may define a magnetic scalar potential Φ_M which satisfies Laplace's equation everywhere inside of the cylinder. Thus,

$$\nabla^2 \Phi_M = 0 \quad (4)$$

and the magnetic field $\mathbf{B} = -\nabla\Phi_M$. In cylindrical coordinates (r, ϕ, z) the components of \mathbf{B} can be expressed as

$$\begin{aligned} B_r &= -\partial\Phi_M/\partial r, \\ B_\phi &= -(1/r)\partial\Phi_M/\partial\phi, \\ B_z &= -\partial\Phi_M/\partial z. \end{aligned} \quad (5)$$

In finding f we never explicitly write \mathbf{B} but work directly with Φ_M . However, to determine Φ_M we use the boundary condition that $B_r = 0$ everywhere on the surface of the cylinder ($r = A$) except at the location of the vortex. The field penetrates the wall only at the vortex location.

Using separation of variables in cylindrical coordinates two categories of solutions naturally arise—those containing the Bessel functions J and N and those containing the modified Bessel functions I and K . Since the N and the K diverge at the origin, they must have zero coefficients in this case. The former lead to an expression for Φ_M containing a sum of terms of the form

$$J_m(k'_{mn}r/A) \begin{cases} \sin m\phi \\ \cos m\phi \end{cases} e^{-k'_{mn}z}, \quad (6)$$

where k'_{mn} is the n th root of the derivative of the m th Bessel function so that

$$[dJ(k'_{mn}r/A)/dr]_{r=A} = 0.$$

Thus the boundary condition at the shield surface is automatically satisfied and we may write

$$\begin{aligned} \Phi_M(r, \phi, z) &= \sum_{m=0}^{\infty} \sum_{n=1}^{\infty} J_m(k'_{mn}r/A) \\ &\quad \times (A_{mn} \sin m\phi + B_{mn} \cos m\phi) e^{-k'_{mn}z}. \end{aligned} \quad (7)$$

This solution corresponds to a semi-infinite cylindrical volume ($z > 0$) where the total flux entering the cylinder at $z = 0$ is zero and no flux leaves through the walls. If the field is known across the top one may solve for the coefficients A_{mn} and B_{mn} . In any case, since the smallest root is $k'_{11} = 1.8412$, all components of any such field will be attenuated at least as fast as $e^{-1.8412z} \approx 0.16$ per radius of the cylinder. Thus the magnetic fields are exponentially attenuated in both directions away from a field source such as a hole in an infinite cylinder or a localized current distribution within it. This exponential attenuation of all magnetic fields within the cylinder, whether caused by an open end or a hole, allows the substitution of an infinite cylinder for the actual shield in our calculations.

Since we wish to find the field arising from the flux entering the shield at one point, the solution involving Bessel functions is not appropriate because along z either $+\infty$ or $-\infty$ must diverge. Instead, we use the solution formed by a sum of terms which include the modified Bessel functions

$$I_m(kr/A) \begin{cases} \sin m\phi \\ \cos m\phi \end{cases} \begin{cases} \sinh kz/A \\ \cosh kz/A \end{cases}. \quad (8)$$

Now we have a Fourier series over the integer index m in the ϕ coordinate and a Fourier transform over the continuous index k along z . For our numerical calculations we approximate the Fourier transform over the continuous variable k with a Fourier series over an integer variable n . Thus

$$\Phi_M(r, \phi, z) = B_0 \sum_{m=0}^{\infty} \sum_{n=0}^{\infty} \frac{L}{n\pi} [I_m(n\pi r/L) / I'_m(n\pi A/L)] \times F_{mn}(\phi, z), \quad (9)$$

$$F_{mn}(\phi, z) = A_{mn} \sin(m\phi) \sin(n\pi z/L) + B_{mn} \sin(m\phi) \cos(n\pi z/L) + C_{mn} \cos(m\phi) \sin(n\pi z/L) + D_{mn} \cos(m\phi) \cos(n\pi z/L),$$

where the F_{mn} form a two-dimensional Fourier series over the intervals $-L < z < +L$ and $-\pi < \phi < +\pi$. The derivative of I_m at $r=A$ has been explicitly included in the coefficients so that the sum over F_{mn} is the boundary condition for $r=A$, i.e., the actual flux pattern penetrating the wall of the cylinder.

To obtain a smooth periodic solution for our problem, we use an alternating distribution of vortices penetrating the cylinder along the same azimuthal coordinate $\phi=0$. The pattern is shown in Fig. 2 where the periodicity along z is $2L$ and the interval of interest for our problem is $-L/2 < z < +L/2$. Thus if flux enters and exits the cylinder in a small square patch of side $2b$ we define two functions g and h as

$$f(\phi) = \begin{cases} 0 & \text{for } -\pi < \phi < -b/A, \\ 1 & \text{for } -b/A < \phi < +b/A, \\ 0 & \text{for } +b/A < \phi < +\pi, \end{cases}$$

$$g(z) = \begin{cases} -1 & \text{for } -L < z < -L+b, \\ 0 & \text{for } -L+b < z < -b, \\ +1 & \text{for } -b < z < +b, \\ 0 & \text{for } +b < z < L-b, \\ -1 & \text{for } +L-b < z < +L, \end{cases} \quad (10)$$

$$F(\phi, z) = f(\phi)g(z),$$

and for $2\Phi_0$ alternately entering and exiting each patch of area $4b^2$ the constant $B_0 = \Phi_0/2b^2$ has units of magnetic field. By symmetry both g and h are pure cosine series

$$\Phi_M(r, \phi, z) = 4\Phi_0/\pi AL \sum_{n=1,3,5,\dots}^{\infty} \left[\frac{I_0(n\pi r/L)}{(2n\pi/L)I'_0(n\pi A/L)} + \sum_{m=1}^{\infty} \frac{I_m(n\pi r/L)}{(n\pi/L)I'_m(n\pi A/L)} \cos m\phi \right] \cos(n\pi z/L), \quad (12)$$

where we have taken the limit as $b \rightarrow 0$. The numerical calculations of the magnetic scalar potential are based on Eq. (12). The larger we make the ratio L/A the more nearly constant the field will be at $z = \pm L/2$; however, the larger L/A , the more terms we must include in the sums. Thus for any given accuracy there is an optimum. To determine Φ_M to better than one part in a thousand we use $L=5A$ as shown in Fig. 2. Then to reconstruct the solution for the original single-vortex problem we use the axial asymptotic values for the magnetic field: $\pm\Phi_0/\pi A^2$

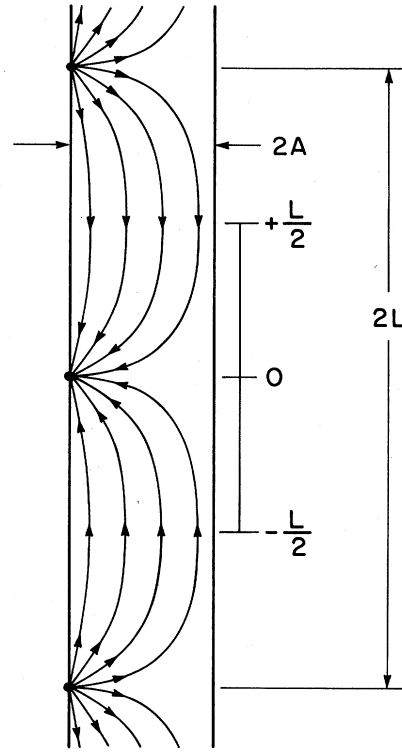


FIG. 2. Schematic representation of trapped fluxon distribution used to compute field inside of cylindrical superconductor.

$$g(\phi) = \frac{2}{\pi} \left[b/2A + \sum_{m=1}^{\infty} (1/m) \sin(mb/A) \cos m\phi \right], \quad (11)$$

$$h(z) = \frac{4}{\pi} \left[\sum_{n=1,3,5,\dots}^{\infty} (1/n) \sin(n\pi b/L) \cos(n\pi z/L) \right],$$

and the two-dimensional Fourier series of F is the product of the one-dimensional series for f and g . Thus we may express the magnetic scalar potential throughout the cylindrical volume over the interval $-L/2 < z < L/2$ as

for $z > L/2$ and $< -L/2$, respectively. This exponential approach to a uniform field is clearly expected from Eq. (7) [the solution in Eq. (7) attenuates to zero, but by superimposing a uniform field the present configuration is generated above the vortex].

The series representation for Φ_M derived in Eq. (12) converges more and more slowly as $r \rightarrow A$. However, we are only interested in finding Φ_M within a radius of $3A/5$ which will always include the largest detector loop of radius $A/2$. Within this restricted volume we found that

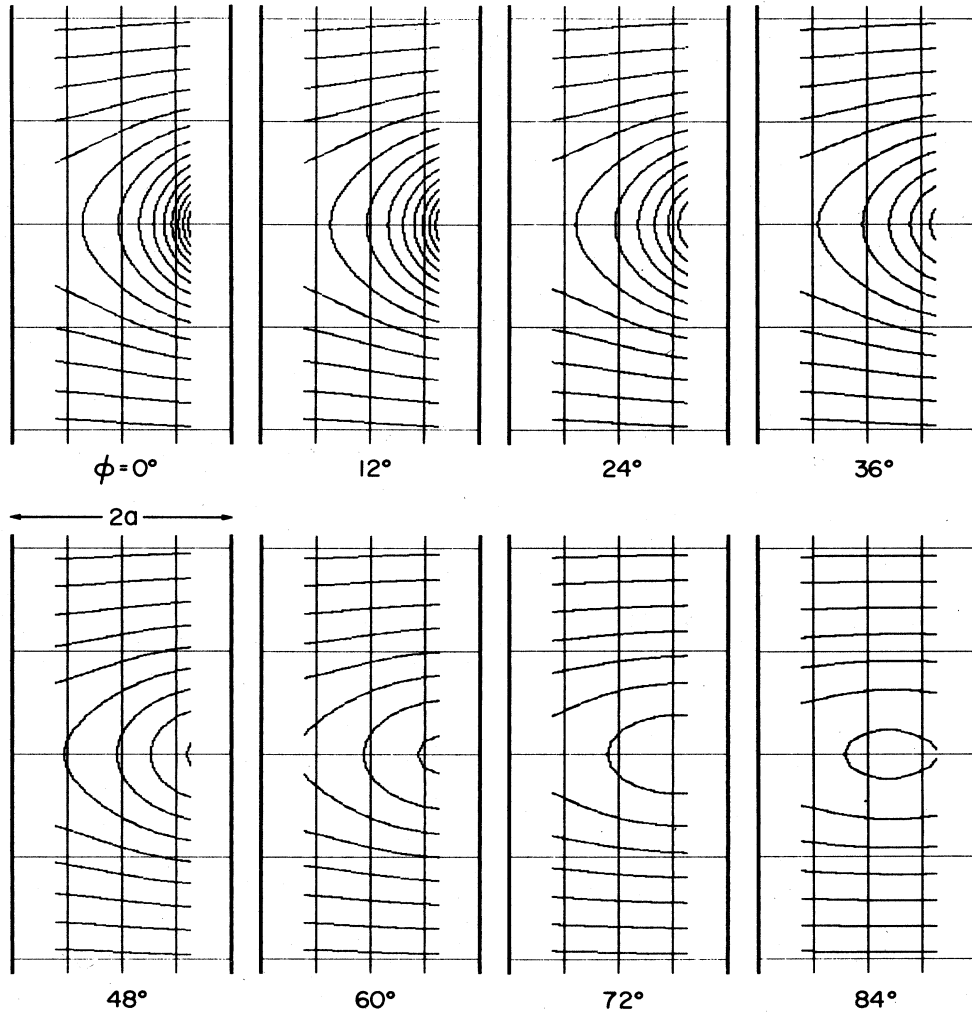


FIG. 3. Magnetic scalar potential inside of cylinder for a doubly quantized fluxon in the shield wall at $\phi = 0^\circ$. The magnetic-field lines are everywhere perpendicular to the constant-potential surfaces shown.

truncation of the sums at $m = 16$ and $n = 31$ maintained an accuracy of better than 1 part in a thousand. We calculated the value of Φ_M on a cylindrical grid of points for $0 < z < L/2$ and $0 < \phi < \pi$, where z and r are spaced at $A/10$ and the ϕ grid has an angular spacing of $\pi/16$. The fourfold symmetry given by $\Phi_M(-z) = \Phi_M(z)$ and $\Phi_M(-\phi) = \Phi_M(\phi)$ allows calculation of four times fewer points. The results of these calculations are plotted in Fig. 3 where eight planes spaced 12 degrees apart are shown. The lines represent constant Φ_M surfaces and the difference in Φ_M for adjacent lines is

$$(A/6)\Phi_0/\pi A^2 = \Phi_0/6\pi A.$$

Before computing the coupling of this field distribution with the various superconducting detector loops, we note that any field distribution inside of a superconducting cylinder can be written as the superposition of many identical field patterns corresponding to the penetration of unit flux at different locations on the cylinder surface. Thus

$$\Phi_{M \text{ tot}}(r, \phi, z) = -N(z/2)\Phi_0/(\pi A^2) + \sum_{i=1}^{\infty} (M_i/2)\Phi_M(r, \phi - \phi_i, z - z_i), \quad (13)$$

where we have taken a distribution of singly quantized vortices located at positions (ϕ_i, z_i) and of polarity $M_i = +1$ (vortex field in) or -1 (vortex field out) on the cylinder surface. A negative or positive integer N represents the net number of flux quanta threading the axis of the cylinder (positive sense represents an upwardly pointing field). Thus Φ_M may be thought of as the Green's function for generating the magnetic scalar potential within the cylinder for a given distribution of surface vortices.

IV. VORTEX-FLUX COUPLING TO LOOPS

We could directly use the three-dimensional Φ_M magnetic scalar potential lookup table to compute the field distribution from an arbitrary monopole trajectory, and

then integrate over the surface of the loops to find the flux coupling. However, it is much more efficient to carry out these time-consuming surface integrals only once and store them in a second lookup table which represents the flux coupling through each detector loop for a vortex placed on a two-dimensional grid of locations on the surface of the cylinder. Then the coupling of an arbitrary trajectory can be found by subtracting the flux coupling from the outgoing vortex from that of the incoming vortex along the trajectory. This technique is used below in the Monte Carlo calculations which generate the sensing-area distribution functions.

To generate this flux lookup table we require the integration of the magnetic-field component normal to the plane of the loop over the surface of the loop. Thus

$$F_{\text{loop}}(\phi, t) = \int_s \mathbf{B} \cdot \hat{\mathbf{n}} da \quad (14)$$

is the flux coupling to the loop from a vortex located at (ϕ, z) with respect to the loop. To perform the integra-

tion, we define a second cylindrical coordination system (q, ψ, h) in which the axial direction h is perpendicular to the plane of the loop. Then

$$F_{\text{loop}}(\phi, z) = \int dq \int q d\psi (-\partial \Phi_M / \partial h), \quad (15)$$

where the normal field component is found by taking the partial derivative of Φ_M along a direction perpendicular to the loop plane. For the numerical calculations, we partition the loop area into a polar grid (we used 128 area elements), each of comparable size to the grid spacing in the Φ_M lookup table and take the derivative by moving above and below the loop a distance of $A/20$ (\pm half the grid spacing). Since the surface-integral area elements are tilted with respect to the Φ_M lookup table, we made extensive use of three-dimensional linear interpolation to find the values of Φ_M for the integration. We first transformed from the coordinates (q, ψ, h) back to the original (r, ϕ, z) and then found Φ_M at an arbitrary point through the relation

$$\begin{aligned} \Phi_M(r, \phi, z) = & [(r - r_i)(\phi - \phi_j)(z - z_k)\Phi_M(r_{i+1}, \phi_{j+1}, z_{k+1}) + (r - r_i)(\phi - \phi_j)(z_{k+1} - z)\Phi_M(r_{i+1}, \phi_{j+1}, z_k) \\ & + (r - r_i)(\phi_{j+1} - \phi)(z - z_k)\Phi_M(r_{i+1}, \phi_j, z_{k+1}) + (r - r_i)(\phi_{j+1} - \phi)(z_{k+1} - z)\Phi_M(r_{i+1}, \phi_j, z_k) \\ & + (r_{i+1} - r)(\phi - \phi_j)(z - z_k)\Phi_M(r_i, \phi_{j+1}, z_{k+1}) + (r_{i+1} - r)(\phi - \phi_j)(z_{k+1} - z)\Phi_M(r_i, \phi_{j+1}, z_k) \\ & + (r_{i+1} - r)(\phi_{j+1} - \phi)(z - z_k)\Phi_M(r_i, \phi_j, z_{k+1}) \\ & + (r_{i+1} - r)(\phi_{j+1} - \phi)(z_{k+1} - z)\Phi_M(r_i, \phi_j, z_k)] / [(r_{i+1} - r_i)(\phi_{j+1} - \phi_j)(z_{k+1} - z_k)], \end{aligned} \quad (16)$$

where (r_i, ϕ_j, z_k) are the grid points in the lookup table and $r_i < r < r_{i+1}$, $\phi_j < \phi < \phi_{j+1}$, and $z_k < z < z_{k+1}$.

For the prototype detector, the loop is positioned with its plane perpendicular to the cylinder axis. Thus the geometry is azimuthally symmetric and the flux coupling to the single loop $F_p(z) = 2\Phi_0 f_p(z)$ is only a function of z . In Fig. 4 we plot the dimensionless quantity $f_p(z)$ where we have used a point spacing of $A/10$ along z . Note that the maximum and minimum couplings occur for $z \rightarrow \pm \infty$ and have a value $\pm \frac{1}{16}$ which is just the ratio of the area of the loop to that of the cross section of the cylinder.

For the larger three-axis detector the tilted loops break the azimuthal symmetry and now $f(\phi, z)$ depends on ϕ and z . Here we have computed the flux coupling for a two-dimensional grid of points with a spacing of $A/10$

along z , extending out to $4A$ and an angular spacing of $\pi/32$ around ϕ . The resulting table is shown in Fig. 5 where contour lines have been drawn along constant values of $f(\phi, z)$. For $z \rightarrow \pm \infty$ the asymptotic values are now $\pm 1/4\sqrt{3}$ so we have used a line spacing of $1/24\sqrt{3}$ in drawing the contours. The maximum occurs at $\phi = 0$ and $z \approx +A/3$ and has a value of $f_{\text{max}} = 0.246$ with the corresponding minimum at $\phi = \pi$, $z \approx -A/3$, and $f_{\text{min}} = -0.246$. The dotted line in Fig. 5 represents the intersection of the loop plane with the cylinder wall. Note that it does not coincide with the $f = 0$ contour. Therefore, there does exist a small solid angle for trajectories in which the induced-supercurrent change from the wall vor-

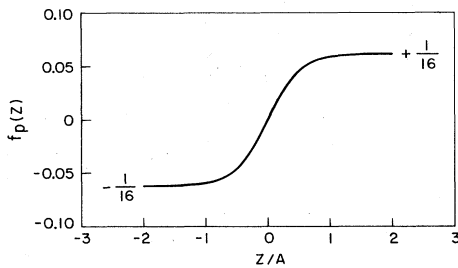


FIG. 4. Fraction $f_p(z)$ of the flux from a trapped fluxon in the shield wall which couples to single-loop-detector geometry. The coupling depends only on the z position of fluxon with respect to loop.

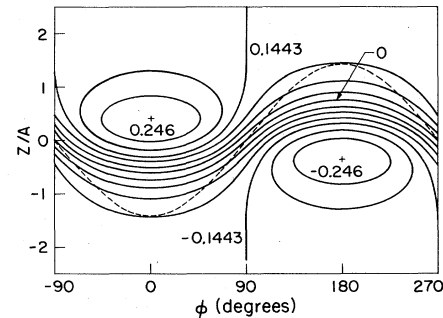


FIG. 5. Contour map of fraction of the flux from a trapped fluxon in the shield wall which couples to one loop of the three-loop detector geometry. The coupling depends on the z and ϕ position of fluxon with respect to the loop.

tices adds to that from the passage through the loop in Eq. (3). Since each of the three loops in this detector has the same tilt angle with respect to the cylinder axis, the flux table is only computed once and we use the following rotation relations to generate f_1 , f_2 , and f_3 for each of loops 1, 2, and 3:

$$\begin{aligned} f_1(\phi, z) &= f(\phi, z), \\ f_2(\phi, z) &= f(\phi - 2\pi/3, z), \\ f_3(\phi, z) &= f(\phi - 4\pi/3, z), \end{aligned} \quad (17)$$

where loops 2 and 3 are rotated by 120 and 240 degrees, respectively, from loop 1. Using these tables we are now ready to set up the Monte Carlo calculations which generate sensing-area functions.

V. SENSING-AREA DISTRIBUTION FUNCTIONS

We are now in a position to compute the total supercurrent change induced by a magnetic charge passing through the detectors along any known trajectory. Utilizing Eq. (3), the task involves defining the trajectory, determining where it enters and exits the cylindrical shield walls so that f_{in} and f_{out} can be found in the lookup tables. We computed the induced supercurrent for a large number of isotropically distributed random trajectories in a Monte Carlo calculation. The results were then compiled to obtain the density of sensing-area distributions as functions of possible induced-current changes. When integrated these provide the total sensing area of the detectors. The density of the sensing area is proportional to the probability of obtaining a particular induced-current change.

To define a straight-line trajectory four independent parameters are needed. We have chosen the spherical angles (θ, ϕ) as defined in Sec. II and the (x, y) coordinates of the intersection of the trajectory with the plane perpendicular to it and which contains the origin. An isotropic distribution is obtained by choosing $\cos\theta$, ϕ , x , and y using uniform random deviates. The distribution of θ values is then weighted as a sine function, as required. The x coordinate is taken to be perpendicular to the trajectory and to the cylinder axis. Only values of x in the interval $(-A, +A)$ need to be used because outside of this range the trajectory does not intersect the cylinder and thus cannot induce a current change. Along the orthogonal direction y , we have chosen an interval $(-15A/4, +15A/4)$ since trajectories outside of this range intersect the cylinder far enough from the loops to induce supercurrents well below the detector noise levels. Each trajectory then corresponds to an effective sensing area integrated over the solid angle given by

$$\Delta\sigma = 15A^2/N_{total}, \quad (18)$$

where N_{total} is the total number of trajectories computed.

Distribution function for single-loop detector

The calculation for the single-loop detector is easier since the detector geometry is azimuthally symmetric and there is only one loop. The randomly generated trajec-

tories only depend on θ , x , and y . For each trajectory, first it is determined whether it passes through the loop ($\eta = +1, -1$) or misses ($\eta = 0$). Sighting along a trajectory at incoming angle θ the loop appears as an ellipse with its normal tilted away through θ . Thus the area through the loop in the x - y plane is the region

$$x^2 + y^2/\cos^2\theta \leq (A/4)^2, \quad (19)$$

where the semimajor axis is always along x and equal to $A/4$.

Finding the flux coupling to the loop from the wall vortices requires determining the z coordinate along the wall for the entering and exiting vortices

$$z_{in/out} = (A/\sin\theta)\{y/A \pm \cos\theta[1 - (x/A)^2]^{1/2}\} \quad (20)$$

and then finding f_{in} and f_{out} by linear interpolation of the single-loop table for f_p , shown graphically in Fig. 4. For the single-loop detector, $N=4$ and $-\frac{1}{16} < f_p < +\frac{1}{16}$, so Eq. (3) shows that all possible induced-supercurrent changes must have a magnitude between 0 and $0.5\Phi_0/L$ if the trajectory misses the loop ($\eta=0$) and between 7.5 and $8\Phi_0/L$ if it passes through ($\eta=\pm 1$). In Fig. 6 we show the results of a calculation using 100 000 isotropically distributed trajectories. Since the distribution is symmetric about zero only the positive values of the induced changes are plotted. The number of trajectories resulting in a particular induced supercurrent was accumulated in an array of bins, each $0.01\Phi_0/L$ wide. In the figure we have normalized the values along the y axis by first converting to sensing area per bin using Eq. (18) and then dividing by the bin width. Thus a density of sensing area in units of $\text{cm}^2 L/\Phi_0$ is obtained.

In Fig. 6 it is seen that the sensing-area density diverges for induced-current changes of 0, 0.5, and $7.5\Phi_0/L$, making these values the most probable. The divergence at zero is not integrable and results from our model of an infinitely long cylinder. However, a natural lower cutoff is provided by the detector noise level. The divergences at 0.5 and $7.5\Phi_0/L$ result from the superconducting shield producing a nearly exact axial field for any trajectory that is approximately axially aligned. Those that miss the loop result in the former value whereas those that pass through result in the latter. Both of these divergences are integrable and the total sensing area averaged over solid angle for trajectories passing through the loop is 10.1 cm^2 (half of the area of the loop $= \frac{1}{2}\pi A^2/16$ as obtained from

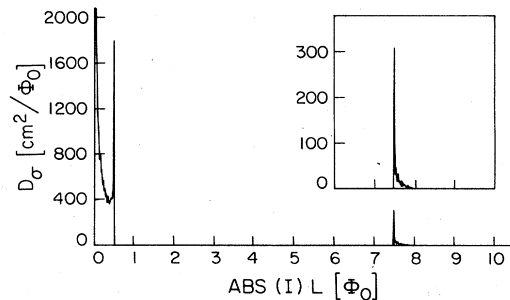


FIG. 6. Sensing-area distribution function vs signal amplitude for single-loop detector.

averaging over the solid). For near-miss events greater than $0.2\Phi_0/L$ the total area is 145 cm^2 . For an isotropic distribution the probability of an event with magnitude between 0.2 and $0.5\Phi_0/L$ is about 15 times greater than for one between 7.5 and $8\Phi_0/L$.

Distribution functions for three-loop detector

For the three-loop detector the loops are tilted, breaking the azimuthal symmetry, and each loop has two turns. Thus in Eq. (3), $N=2$ and f_{in} and f_{out} have a range of values between $-0.25 \leq f \leq +0.25$. For trajectories which miss the loop the range of possible induced supercurrent changes is from 0 to $1\Phi_0/L$ and those that pass through range from 3 to $4.4\Phi_0/L$. The maximum flux response for each loop in this detector is somewhat larger than $4\Phi_0/L$ as discussed in Sec. IV.

Determining whether or not the trajectory intersects the tilted loops requires a tedious but straightforward calculation. As seen from a line along the monopole trajectory (θ, ϕ) the loop appears as an ellipse with its normal tilted away from the line of sight through an angle α and its projection rotated counterclockwise through an angle β away from the cylinder axis projection. Thus,

$$\cos\alpha = \cos\theta_0 \cos\theta + \sin\theta_0 \sin\theta \cos\phi, \quad (21)$$

$$\cos\beta = (\cos\theta_0 - \cos\alpha \cos\theta) \sin\theta \sin\alpha,$$

where the cube diagonal angle $\theta_0 = \cos^{-1}(1/\sqrt{3})$. A relation similar to Eq. (19) is obtained to define the loop area for this case:

$$x'^2 + y'^2 / \cos^2\alpha \leq (A/2)^2, \quad (22)$$

where

$$x' = x \cos\beta + y \sin\beta, \quad (23)$$

$$y' = -x \sin\beta + y \cos\beta.$$

The semimajor axis is always $A/2$. The vortex wall positions are determined for each trajectory through Eq. (20) for z_{in} and z_{out} and for ϕ_{in} and ϕ_{out} using

$$\phi_{\text{in}} = \phi + \arctan\{(x/A)/[1-(x/A)^2]^{1/2}\}, \quad (24)$$

$$\phi_{\text{out}} = 2\phi + \pi - \phi_{\text{in}}.$$

These are used to determine f_{in} and f_{out} from the flux lookup table for the tilted loop (Fig. 5). Two-dimensional linear interpolation is used and can be derived from Eq. (16) by setting $r=r_i$ and replacing Φ_M everywhere with f .

The sensing-area density is identical for all of the three loops and is shown in Fig. 7 plotted against the induced-supercurrent change. Again 100 000 trajectories were used and the absolute value of the induced changes is plotted. Now divergences occur at 0 , $0.5774 = \cos\theta_0$, and $3.4226 = 4 - \cos\theta_0$ in units of Φ_0/L . Again the first divergence is not integrable and results from the use of an infinite cylinder. However, the detector noise level at $0.1\Phi_0/L$ provides a natural lower cutoff. The other two divergences are integrable and, as was the case with the single-loop detector, are due to the field from approxi-

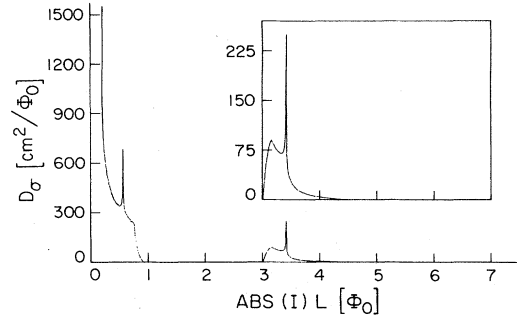


FIG. 7. Sensing-area distribution function vs signal amplitude for one loop of the three-loop detector.

mately axial trajectories resulting in nearly an exact axial field at the loop. The total sensing area for trajectories through the coil, $40.4 \text{ cm}^2 (= \frac{1}{2}\pi A^2/4)$, is obtained by integrating between 3 and $4.4\Phi_0/L$ in Fig. 7 as expected. In this detector the coils are tilted so that the divergences no longer occur at the ends of the allowed induced-current ranges.

Since the response of the three loops are highly correlated, the one-loop distribution function shown in Fig. 7 does not characterize the detector response. Instead it is necessary to define a four-dimensional phase space in which the response of each loop is taken as an axis and the sensing-area magnitude, taken as the fourth dimension, defines the distribution function. To compute this function we used an isotropic distribution of trajectories limited in solid angle to $0 < \theta < \pi/2$ and $0 < \phi < \pi/3$. The 12-fold symmetry of the detector then allows 12 points in the phase space to be generated through symmetry relations. Thus for computed induced-current changes of I_a , I_b , and I_c in loops 1, 2, and 3, the induced changes for the 12 symmetric trajectories are $\pm(I_a, I_b, I_c)$, $\pm(I_b, I_a, I_c)$, $\pm(I_c, I_a, I_b)$, $\pm(I_c, I_b, I_a)$, $\pm(I_b, I_c, I_a)$, and $\pm(I_a, I_c, I_b)$, where the six '+'s correspond to reflection through the origin of the '-'s.

A random array of 1 000 000 trajectories was used and the induced-three-loop current changes were computed for each one. A three-dimensional array of bins each $0.1\Phi_0/L$ on an edge was used to count the number of trajectories producing that particular three-loop current change. Each trajectory generated 12 entries for a total of 12 000 000. To visualize this function a contour plot in three dimensions can be drawn as shown in Fig. 8. We have taken slices through the three-dimensional space each perpendicular to the third-loop axis. Rather than drawing contour lines, we have shaded the areas according to the density of phase space at that point. Different shading was used to divide the sensing-area densities into four groups containing equal total numbers of trajectories. From lightest to darkest, these correspond to sensing-area densities of 0 to 5.9 , 5.9 to 31.0 , 31.0 to 128.5 , and greater than $128.5 \text{ cm}^2 / \langle \Phi_0/L \rangle^3$, respectively.

The central core is caused by the trajectories that missed all of the loops but passed through the shield. The cup-shaped regions in the faces of the cubes hit exactly one of the loops, those along the edges hit exactly two

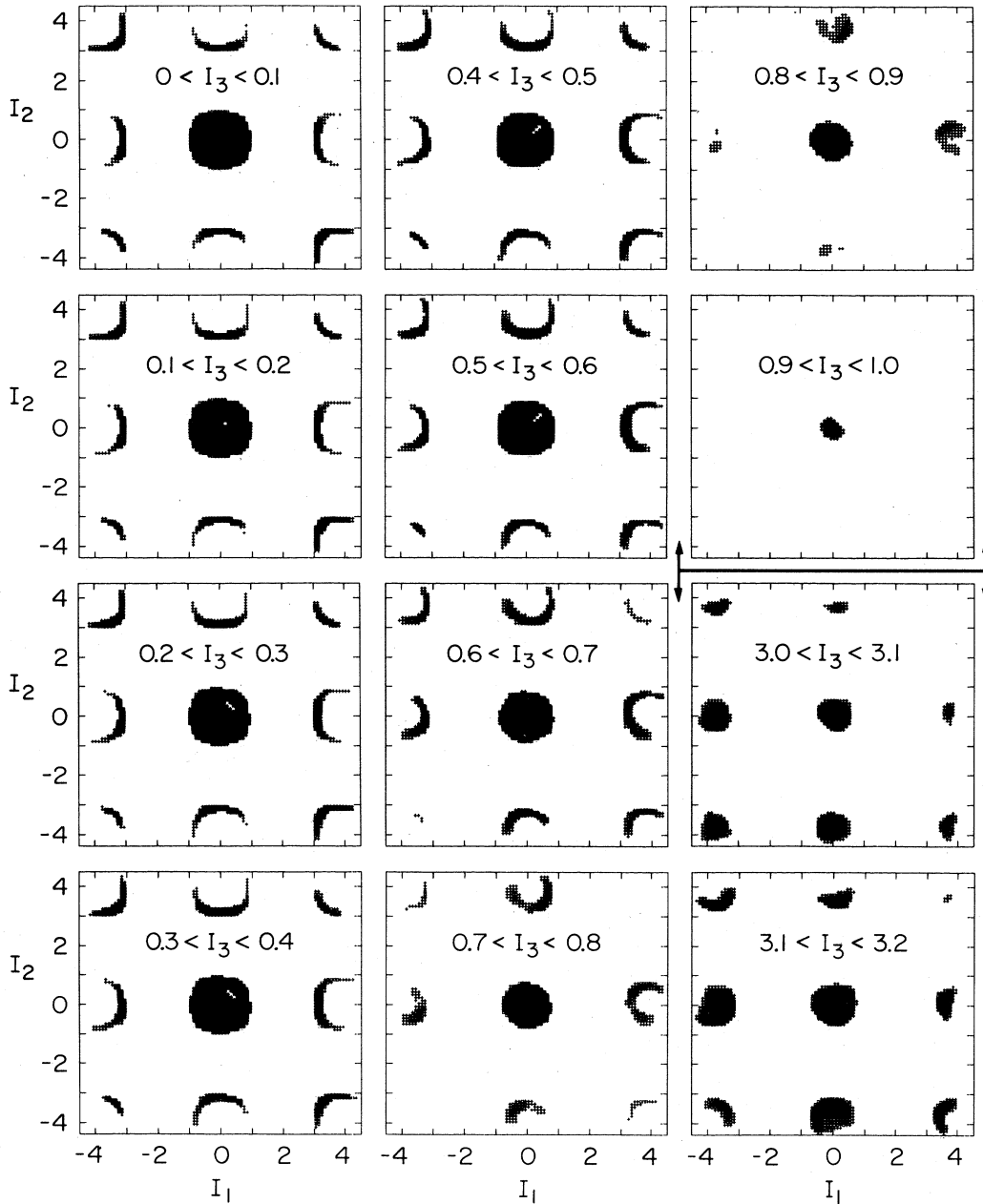


FIG. 8. Three-dimensional sensing-area distribution function versus simultaneous signal levels in all three loops of the three-loop detector.

loops, and those in the corners hit all three loops. The hole in the central core corresponds to a region on the cylinder where a coupling of that magnitude can only occur for trajectories that also hit at least one loop. Less than 1% of the phase-space volume outside of the central core contains nonzero density, providing good discrimination for identification of magnetic-charge candidates.

The three-loop distribution function can be folded into one dimension by plotting sensing-area density against the three-loop magnitude ΔI_{mag} defined as

$$\Delta I_{\text{mag}} = [(\Delta I_1)^2 + (\Delta I_2)^2 + (\Delta I_3)^2]^{1/2}. \quad (25)$$

The resulting one-dimensional distribution is shown in Fig. 9(a). The high densities from 0 to $1\Phi_0/L$ are due to trajectories that miss the loops and the three separated peaks correspond to trajectories that hit exactly one, two, or three loops in order of increasing magnitude. Divergences again occur at $0\Phi_0/L$ from the infinite cylinder and at

$$\begin{aligned} 1.0000\Phi_0/L &= [3(1/\sqrt{3})^2]^{1/2}\Phi_0/L, \\ 3.5187\Phi_0/L &= [2(1/\sqrt{3})^2 + (4-1/\sqrt{3})^2]^{1/2}\Phi_0/L, \\ 4.8747\Phi_0/L &= [(1/\sqrt{3})^2 + 2(4-1/\sqrt{3})^2]^{1/2}\Phi_0/L, \\ 5.9282\Phi_0/L &= [3(4-1/\sqrt{3})^2]^{1/2}\Phi_0/L \end{aligned} \quad (26)$$

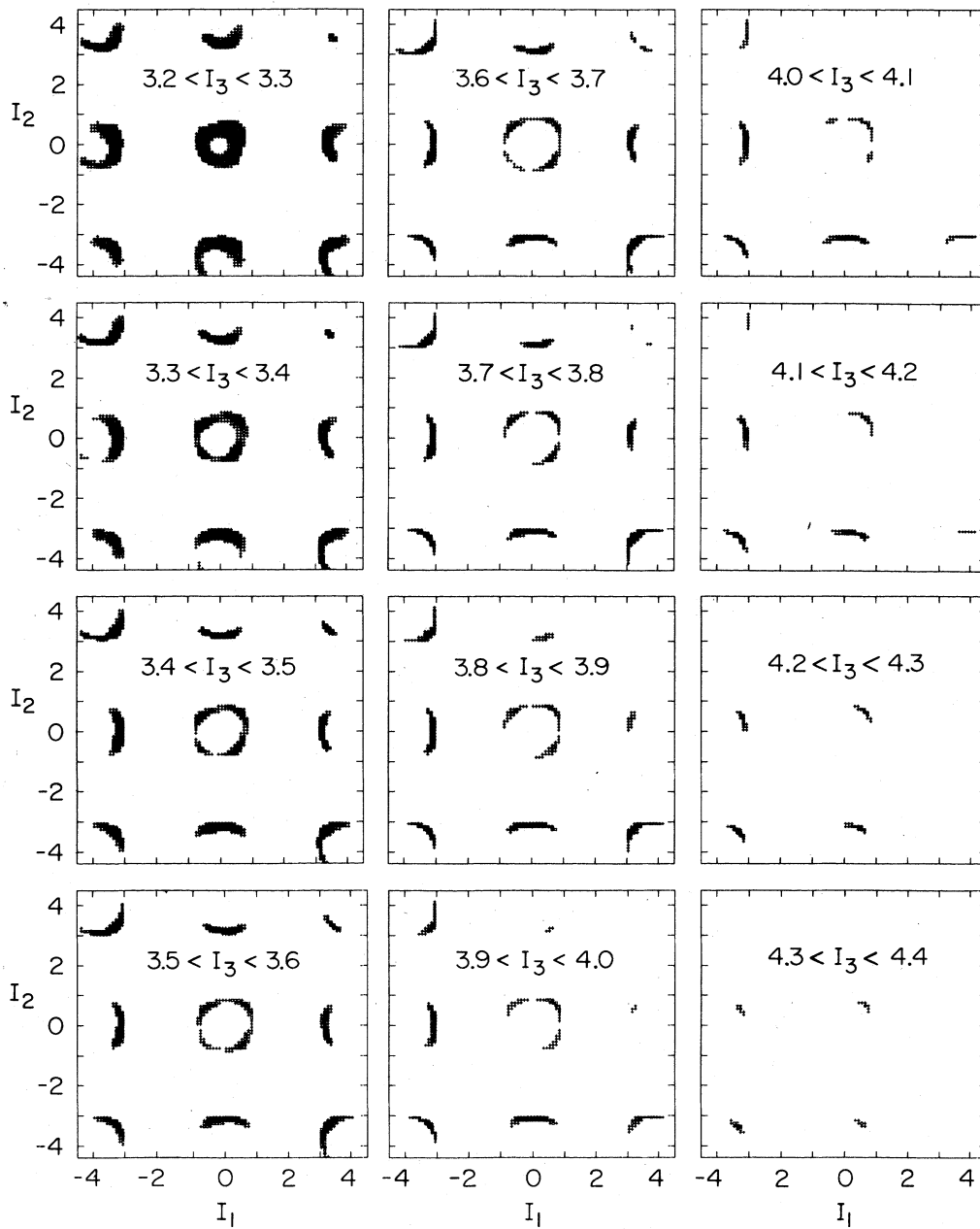


FIG. 8. (Continued).

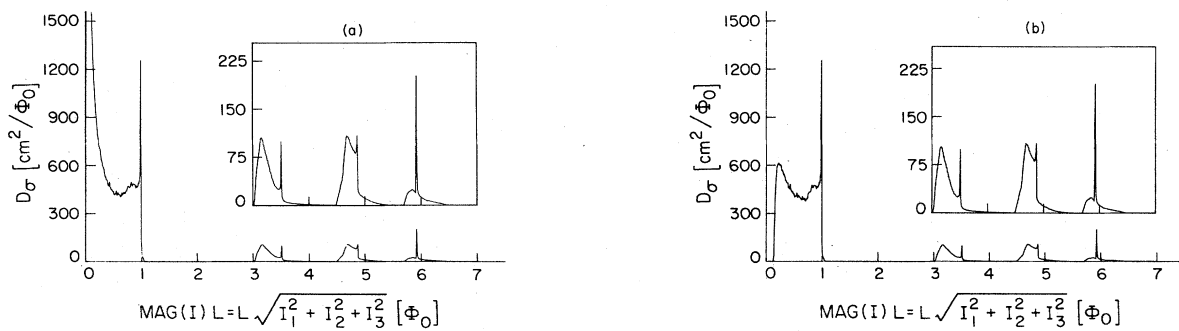


FIG. 9. Sensing-area distribution function versus the three-loop signal magnitude for the three-loop detector with (a) no coincidence requirement and (b) double coincidence required.

for the approximately axial trajectories which miss all three loops or hit exactly one, two, and three loops, respectively. As before, all but the one at 0 are integrable. The areas under each of the three peaks are 30.3, 30.3, and 10.1 cm², respectively, and correspond to the total sensing area averaged over solid angle for those trajectories which hit exactly one, two, or three loops. The total sensing area for all events with magnitude greater than $0.1\Phi_0/L$ is 601 cm².

An independent calculation has shown that for these three mutually orthogonal loops which lie on the surface of a sphere of radius equal to the loop radii $A/2$ the sensing areas under the three peaks should be exactly $\frac{3}{8}S$, $\frac{3}{8}S$, and $\frac{1}{8}S$, respectively, where $S = \pi(A/2)^2 = 81.1$ cm² is the area of each loop. The total sensing area for trajectories that pass through one or more loops is $\frac{7}{8}S = 70.8$ cm². All of these numbers are in agreement within the statistical uncertainties of the Monte Carlo-calculation results shown in Figs. 8 and 9(a).

The large signals caused by any event which passed through at least one loop would have a high confidence level and the phase-space discrimination discussed above would strengthen the confidence. However, the near-miss sensing area is about a factor of 7 larger than that for the loops themselves and it is thus important to utilize it as much as possible. One way to improve the confidence level for the near-miss events is to require that two or even all three loops simultaneously register supercurrent changes greater than $0.1\Phi_0/L$. The effect of these coincidence requirements on the detector sensitivity can also be obtained from the three-loop distribution function shown in Fig. 8. Taking out the cube around zero with edges -0.1 to $+0.1\Phi_0/L$ along each axis leaves all remaining events with at least one loop above a threshold of $0.1\Phi_0/L$. The resulting total sensing area of 601 cm² has already been discussed and it is shown in Fig. 9(a).

The requirement for double coincidence has the effect of removing a square cross-section tube with -0.1 to $+0.1\Phi_0/L$ for each width from along each axis. The resulting folded one-dimensional distribution function is shown in Fig. 9(b). The total sensing area is reduced to 476 cm² primarily from elimination of the low-magnitude tail. There is also a negligible reduction in the size of the first peak and no effect on the second two peaks. Thus a small number of low-magnitude spurious events occurring in one loop at a time can be successfully removed from consideration using double coincidence.

The most stringent requirement would be for simultaneous triple coincidence above a $0.1\Phi_0/L$ threshold in all loops. This requirement has the effect of removing three orthogonal planes through the coordinate origin. Each plane is normal to an axis and has a thickness from -0.1 to $+0.1\Phi_0/L$. With this requirement the total sensing area is further reduced to 280 cm² and is no longer limited to the low-magnitude tail but also extends throughout the near-miss category and significantly reduces both of the first two peaks leaving only the third unaffected. Unless a very large number of low-magnitude spurious signals were seen, which has not been the case, this more severe triple coincidence would not be necessary.

Should interesting candidate events be seen, the question of the directionality information provided by this detector would be important. To address this question, we have run several Monte Carlo simulations, where we store the trajectory direction (θ, ϕ) on all trajectories that produce a preselected detector response (within a $0.1\Phi_0/L$ cube in the phase space shown in Fig. 8). These trajectories are best displayed on a polar coordinate plot where the center is the direction of the vector sum of all trajectories. The results for a typical event passing through at least one loop, and for a near-miss event are shown in Figs. 10(a) and 10(b), respectively. It is not possible to distinguish a positive charge moving one way along a tra-

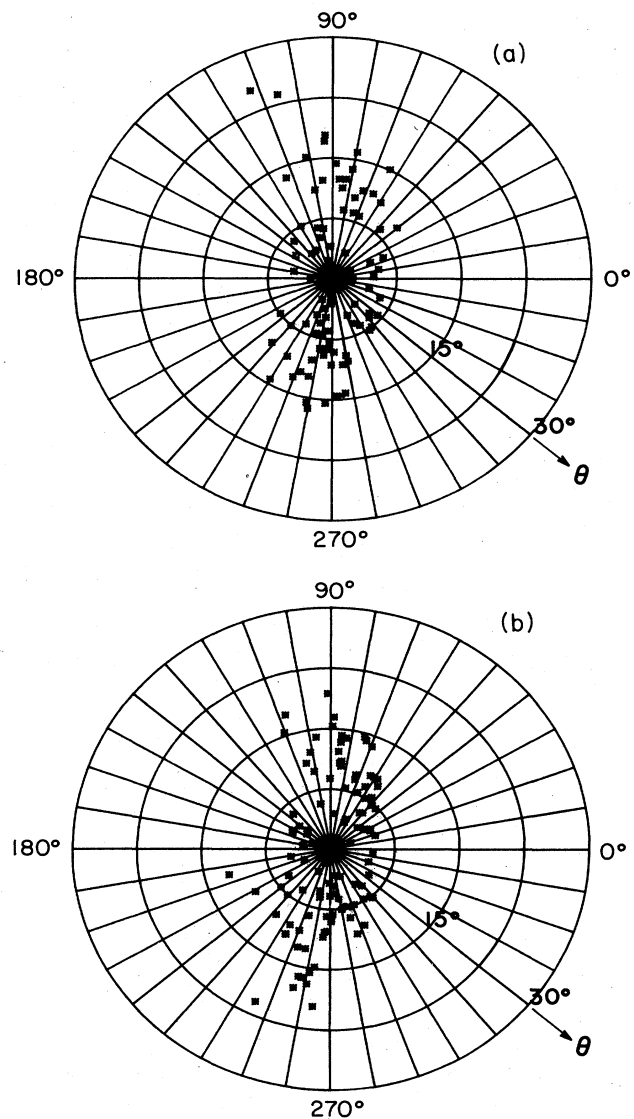


FIG. 10. Angular distribution of trajectories which produce the same simultaneous three-loop event for (a) a typical direct-loop event with $I_1L = 3.3\phi_0$, $I_2L = -0.6\phi_0$, and $I_3L = 3.4\phi_0$ and (b) for a typical near-miss event with $I_1L = 0.3\phi_0$, $I_2L = -0.3\phi_0$, and $I_3L = 0.2\phi_0$. The center of each plot is the average direction of the distribution. The azimuthal angle is ϕ .

jectory with a negative moving in the opposite direction. The information on directionality is better than we had expected, particularly for near-miss events which provide an angular resolution about equal to that from loop events. In general a given three-loop signal can only be produced by trajectories within a 15-degree half-angle cone of the mean direction producing that detector response.

VI. CONCLUSIONS

We have completely characterized the response of the prototype single-loop and the larger three-loop superconductive detectors to an isotropic flux of magnetic monopoles. Only the portion of the detector shields within one diameter above and below the sensing loops contributes to the signal due to the exponential attenuation of magnetic-field sources within superconducting cylindrical shields. Our idealized detector models, which use infinite cylindrical shields are thus an excellent approximation. Uncer-

tainties in the actual dimensions of our physical detectors ($\pm 1\%$) introduce errors no greater than $\pm 0.1\Phi_0/L$, plus or minus one bin in the sensing-area distribution functions. The numerical results throughout this paper were confirmed by independent calculations obtained on a separate computer with codes written in a different computer language. The mathematical techniques (particularly in Secs. III and IV) are applicable to the solution of a large class of magnetic-field boundary-value problems with superconducting shields with cylindrical symmetry. Should interesting candidate events appear during the continuing operation of the three-loop detector, the distribution functions from these calculations would contribute discrimination between real and spurious signals.

ACKNOWLEDGMENT

The work presented in this paper was supported in part by Department of Energy Contract No. DE-AM03-76-SF00326 and National Science Foundation Grant No. DMR80-26007.

¹For a recent detailed review of theory and experiment, see *Magnetic Monopoles*, edited by R. A. Carrigan and W. P. Trower (Plenum, New York, 1983).

²B. Cabrera, *Phys. Rev. Lett.* **48**, 1378 (1982).

³B. Cabrera, M. Taber, R. Gardner, and J. Bourg, *Phys. Rev. Lett.* **51**, 1933 (1983).